Extended Data Fig.1

a

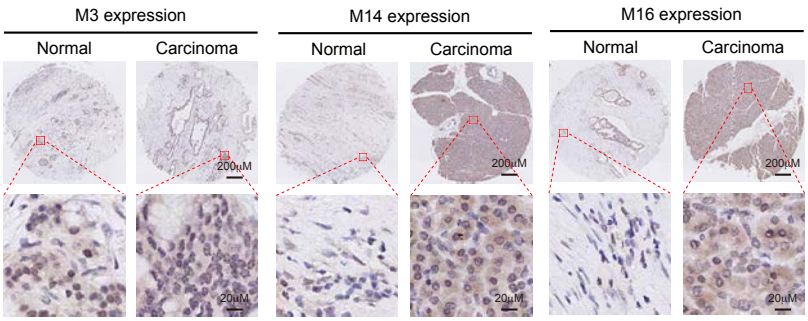

b

Correlation of M3/M14/M16 expression between normal and carcinoma tissues (n= 150)

		specimens		*p* value
		Normal (40)	Carcinoma (110)	
M3	Low (77)	18	59	0.3494
	High (73)	22	51	
M14	Low (63)	25	38	0.0022
	High (87)	15	72	
M16	Low (59)	24	35	0.0018
	High (91)	16	75	

c

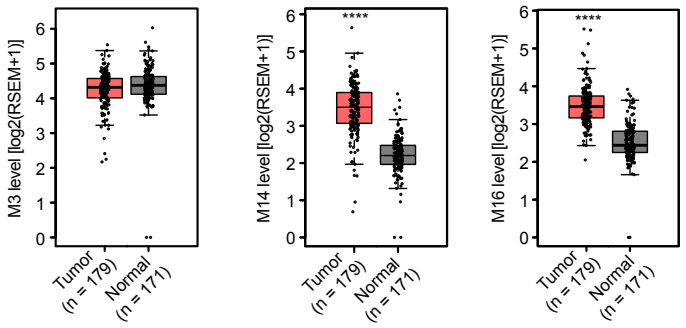

e

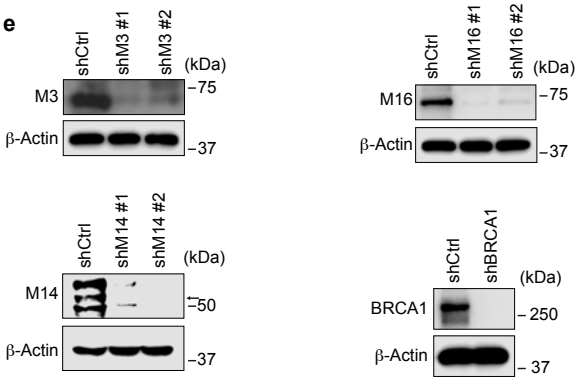

d

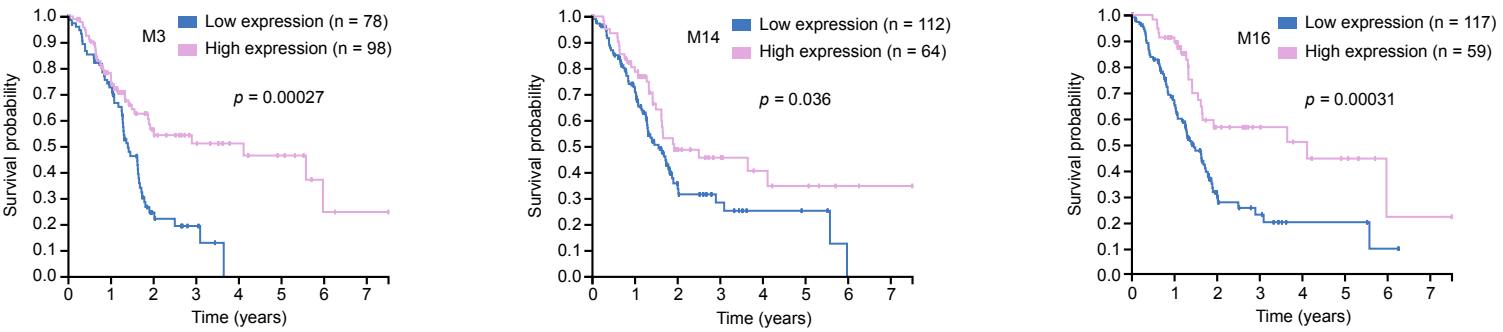

Extended Data Fig. 1 Elevated METTL16 expression indicates favorable outcomes in PDAC. a, Representative IHC micrographs showing METTL3, METTL14, and METTL16 expression in normal and carcinoma tissues in the microarray, respectively. Scale bars are indicated. **b,** Correlation of METTL3, METTL14, and METTL16 expression level between normal and carcinoma tissues. Protein levels of METTL3, METTL14, and METTL16 were quantified in tissue microarrays from PDAC and normal specimens (χ^2 test; p value are indicated). **c,** Expression level of METTL3, METTL14, and METTL16 in normal and carcinoma tissues of PDAC in GEPIA (Gene Expression Profiling Interactive Analysis). (student's t test; ****$p < 0.0001$). **d,** Kaplan-Meier survival curves for overall survival of PDAC patients with low and high expressing METTL3, METTL14, or METTL16 from "The Human Protein Atlas". **e,** Immunoblots of METTL3, METTL14, METTL16, and BRCA1 in HEK293T cells after infected with lentiviruses encoding control shRNA or two different targeting shRNAs. β-Actin was used as a loading control.

Extended Data Fig.2

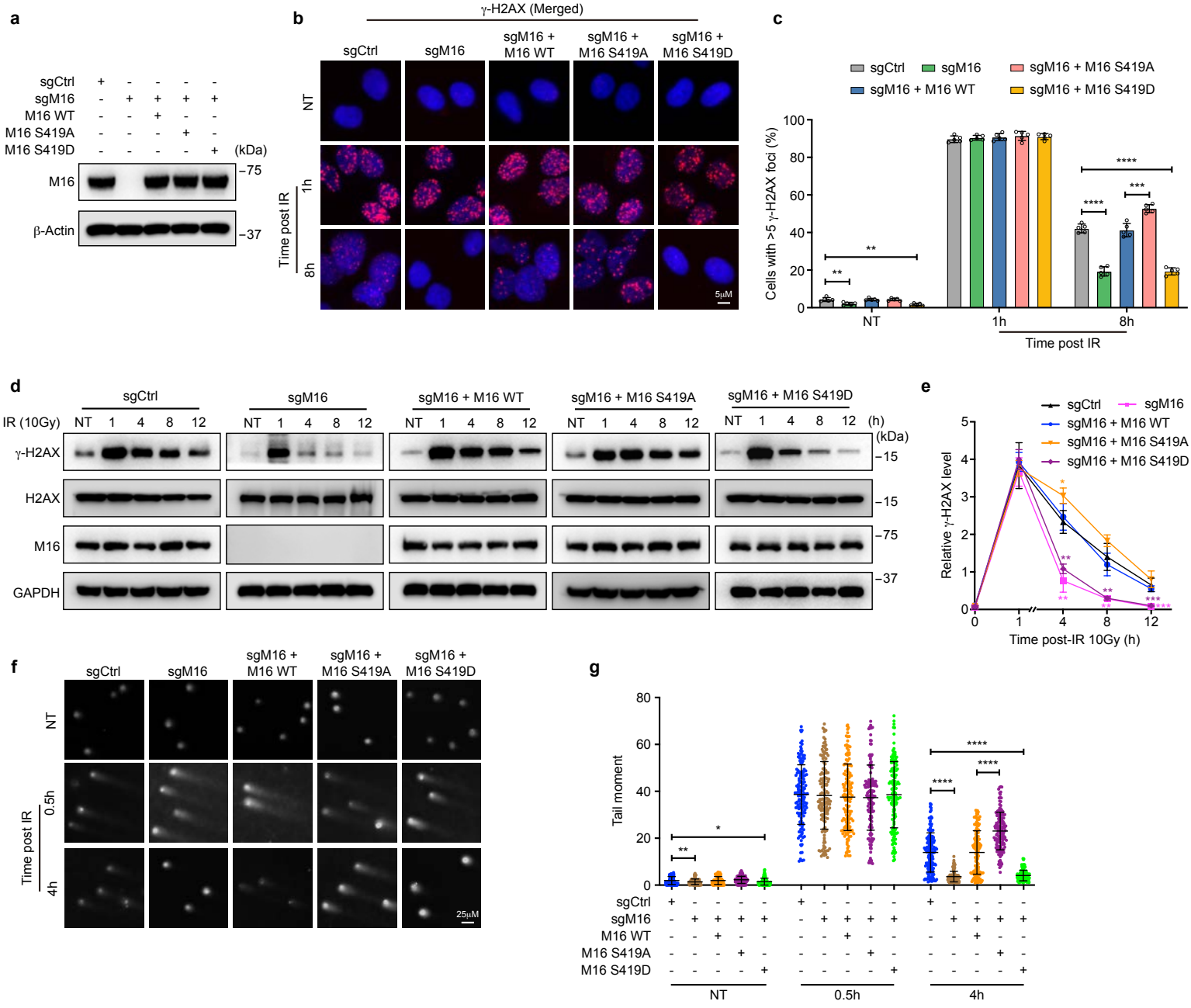

Extended Data Fig. 2 METTL16 suppresses HR regulated by ATM phosphorylation

a, Immunoblot of METTL16 in METTL16 KO U2OS cells expressing METTL16 WT, S419A, or S419D vectors. β-Actin was used as a loading control. **b,c,** Representative images **b** and quantification **c** of γ-H2AX foci formation in the indicated U2OS cells without IR or at 1 h and 8 h after IR with 5 Gy. At least 150 cells were analyzed for each datum point. Data are presented as mean ± SD from five independent experiments (student's t test; $^{**}p < 0.01$, $^{***}p < 0.001$, $^{****}p < 0.0001$). Scale bar is indicated. **d,** Comparison of IR-induced γ-H2AX levels in the indicated U2OS cells. Immunoblot detection of γ-H2AX was collected at the indicated time point after IR with 10Gy. NT, no treatment. **e,** Quantitative analysis of the relative levels of γ-H2AX normalized to H2AX loading control by ImageJ software. Data are presented as mean ± SD from three independent experiments (two-way ANOVA; $^{*}p < 0.05$, $^{**}p < 0.01$, $^{***}p < 0.001$). **f,g,** Representative images **f** and quantification **g** of neutral comet assay in the indicated U2OS cells without IR or at 0.5h, 4h after IR with 5Gy. The tail moment was analyzed using the CometScore software. At least 200 cells were analyzed for each datum point. Data are presented as mean ± SD from five independent experiments (student's t test; $^{*}p < 0.05$, $^{**}p < 0.01$, $^{****}p < 0.0001$). Scale bar is indicated.

Extended Data Fig.3

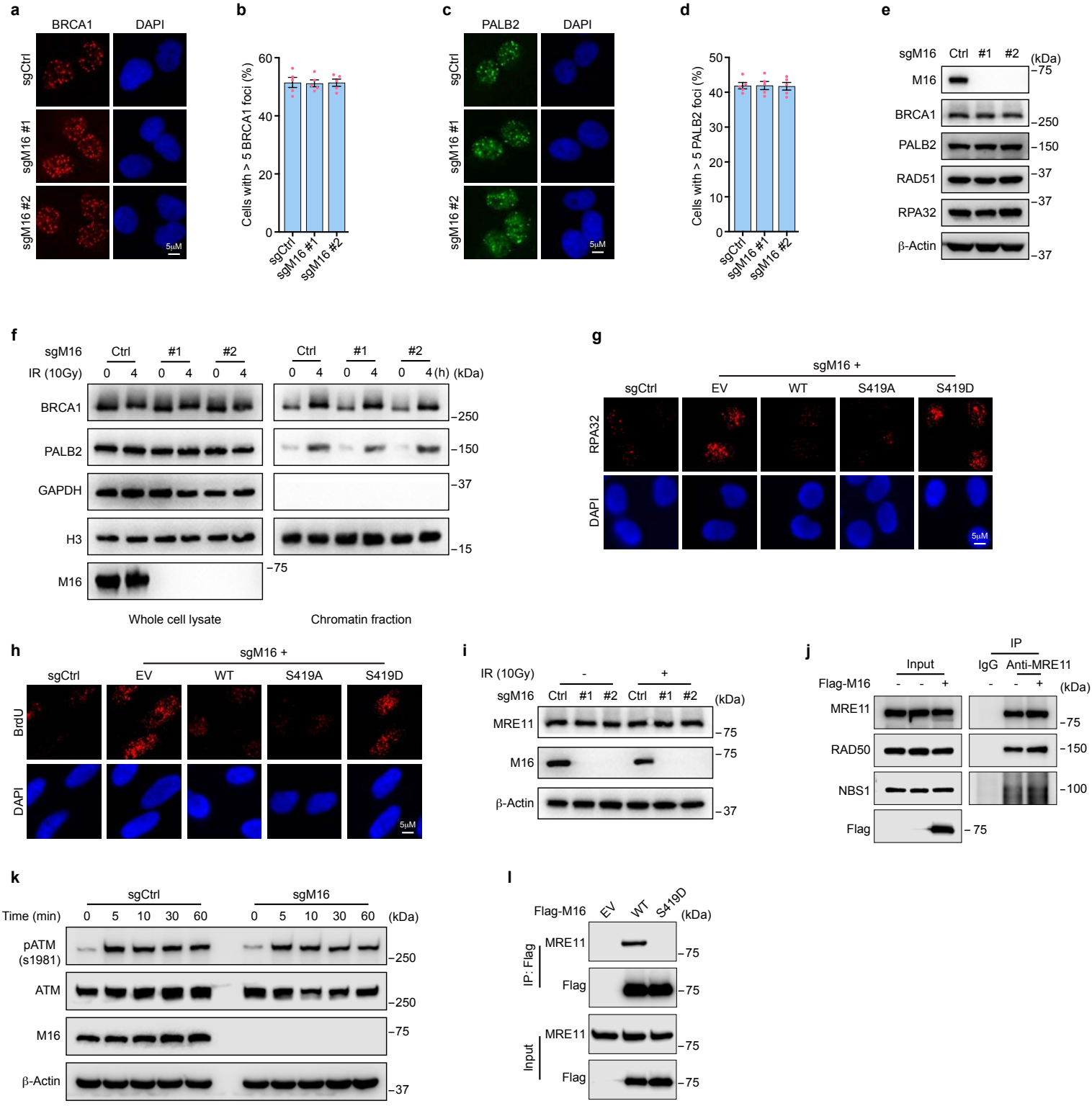

Extended Data Fig. 3 METTL16 inhibits DNA end resection through MRE11. **a-d,** Representative images (**a** and **c**) and quantification (**b** and **d**) of BRCA1, and PALB2 foci in METTL16 KO U2OS cells. Foci are shown at 4 h after IR with 5 Gy. At least 150 cells were analyzed. Data are presented as mean ± SD from five independent experiments (student's t test). Scale bars are indicated. **e,** Immunoblot of indicated antibodies in METTL16 KO U2OS cells. **f,** Western blots with total or chromatin-enriched extracts from indicated U2OS cells without IR or at 4 h after IR with 10 Gy. **g,h,** Representative images of RPA32 **g** and BrdU **h** foci in METTL16 KO U2OS cells expressing METTL16 WT, S419A, or S419D vectors. RPA32 foci are shown at 4 h after IR with 5 Gy. BrdU foci are shown at 1h after IR with 10 Gy. Scale bars are indicated. **i,** Immunoblot of MRE11 and METTL16 in KO METTL16 U2OS cells with or without IR (10 Gy). β-Actin was used as a loading control. **j,** Endogenous IP of MRE11 with RAD50 and NBS1 after transfection with Flag-METTL16 in HEK293T cells. **k,** Immunoblot of pATM (s1981), ATM, and METTL16 at indicated times following 5 Gy IR in METTL16 KO U2OS cells. β-Actin was used as a loading control. **l,** HEK293T cells were transfected with Flag-METTL16 WT or S419D vectors. Cell lysates were subjected to immunoprecipitation with Flag beads and immunoblotted with the indicated antibodies.

Extended Data Fig.4

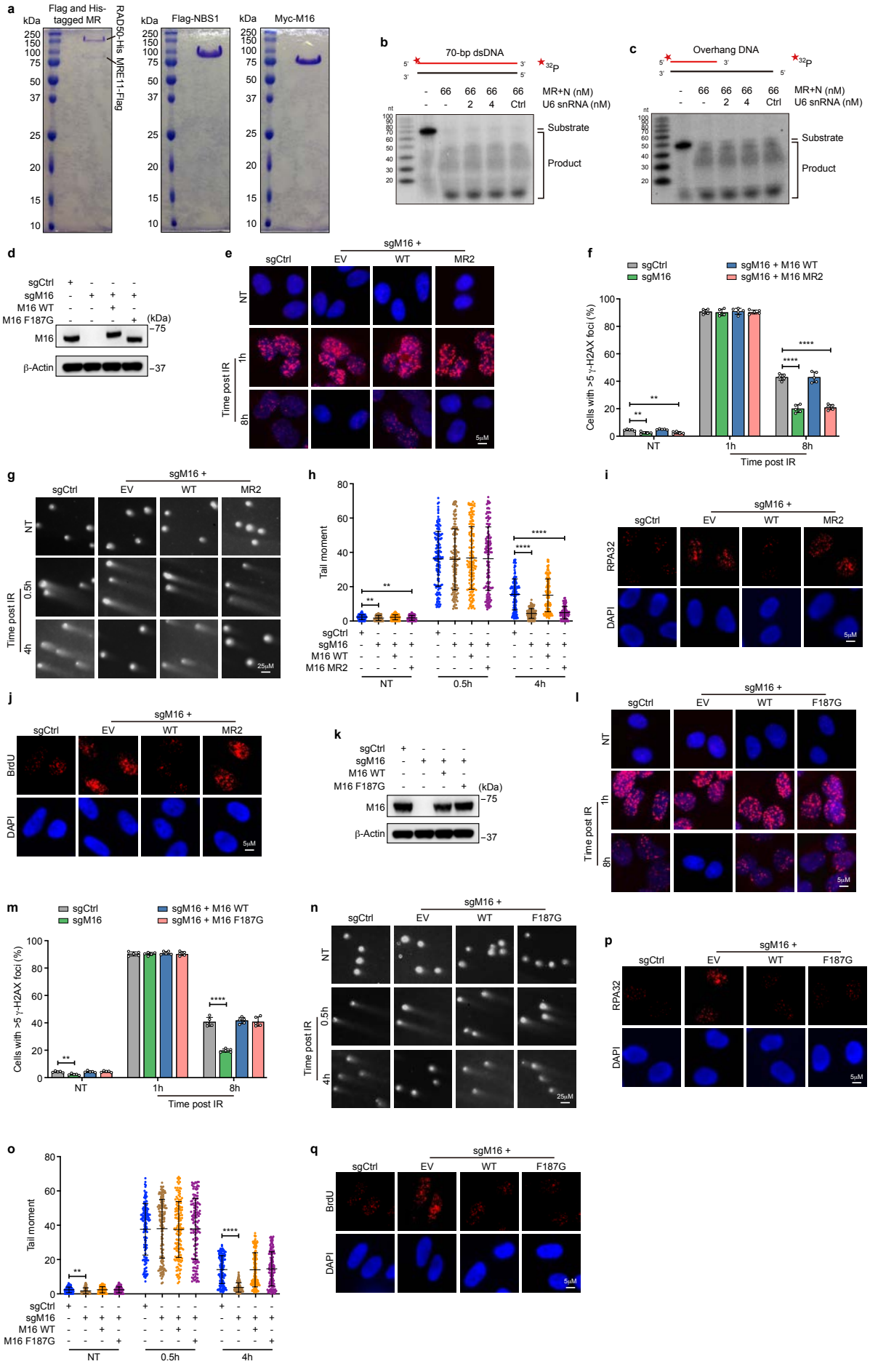

Extended Data Fig. 4 METTL16 inactivates MRE11 by forming METTL16-RNA-MRE11 complex. a, Expression and purification of MRE11/RAD50 (MR), NBS1, and METTL16 proteins *in vitro*. Flag-tagged MRE11 and His-tagged RAD50 were co-expressed. **b,c,** Purified proteins of MRE11, RAD50, NBS1 and control RNA or U6 snRNA were incubated with 5' labeled ^{32}P blunt **b** or overhang **c** DNA substrate *in vitro*. The cleavage products were shown below by autoradiography. **d,** Immunoblot of METTL16 in METTL16 KO U2OS cells expressing WT or MR2 mutant METTL16. β-Actin was used as a loading control. **e,f,** Representative images **e** and quantification **f** of γ-H2AX foci formation in the indicated U2OS cells without IR or at 1 h and 8 h after IR with 5 Gy. At least 150 cells were analyzed for each datum point. Data are presented as mean ± SD from five independent experiments (student's t test; **p < 0.01, ****p < 0.0001). Scale bar is indicated. **g,h,** Representative images **g** and quantification **h** of neutral comet assay in the indicated U2OS cells without IR or at 0.5 h and 4 h after IR with 5 Gy. The tail moment was analyzed using the CometScore software. At least 200 cells were analyzed for each datum point. Data are presented as mean ± SD from five independent experiments (student's t test; *p < 0.05, **p < 0.01, ****p < 0.0001). Scale bar is indicated. **i,j,** Representative images of RPA32 **i** and BrdU **j** foci in METTL16 KO U2OS cells expressing METTL16 WT or MR2 vectors. RPA32 foci are shown at 4 h after IR with 5 Gy. BrdU foci are shown at 1 h after IR with 10 Gy. Scale bars are indicated. **k,** Immunoblot of METTL16 in METTL16 KO U2OS cells expressing WT or F187G mutant METTL16. β-Actin was used as a loading control. **l,m,** Representative images **l** and quantification **m** of γ-H2AX foci formation in the indicated U2OS cells without IR or at 1 h and 8 h after IR with 5 Gy. At least 150 cells were analyzed for each datum point. Data are presented as mean ± SD from five independent experiments (student's t test; **p < 0.01, ****p < 0.0001). Scale bar is indicated. **n,o,** Representative images **n** and quantification **o** of neutral comet assay in the indicated U2OS cells without IR or at 0.5 h and 4 h after IR with 5 Gy.

The tail moment was analyzed using the CometScore software. At least 200 cells were analyzed for each datum point. Data are presented as mean ± SD from five independent experiments (student's t test; *$p < 0.05$, **$p < 0.01$, ****$p < 0.0001$). Scale bar is indicated. **p,q,** Representative images of RPA32 **p** and BrdU **q** foci in METTL16 KO U2OS cells expressing METTL16 WT or F187G vectors. RPA32 foci are shown at 4 h after IR with 5 Gy. BrdU foci are shown at 1 h after IR with 10 Gy. Scale bars are indicated.

Extended Data Fig.5

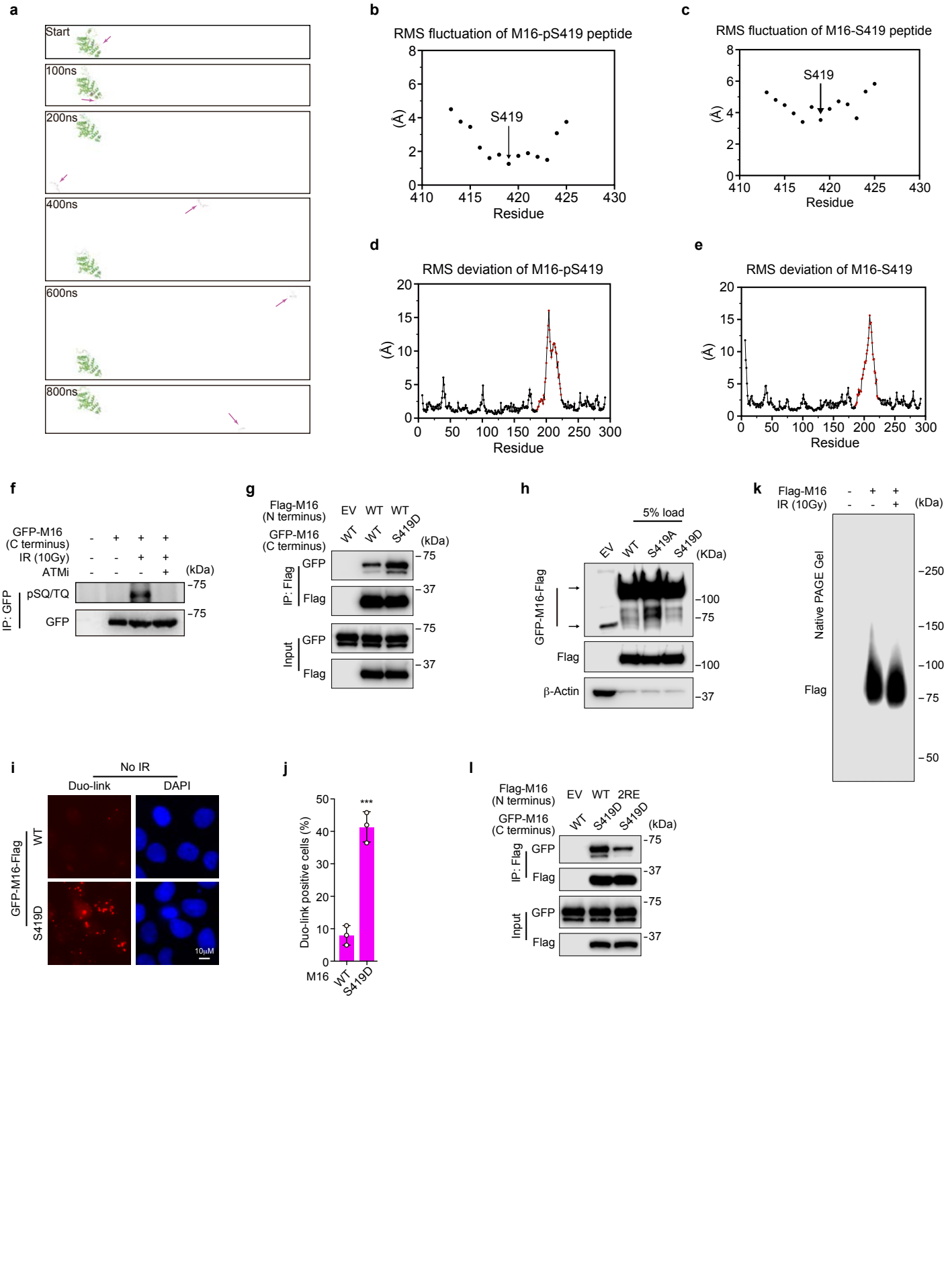

Extended Data Fig. 5 METTL16 phosphorylated at Ser419 induces conformational change and autoinhibited for RNA binding. a, The unmodified METTL16 peptide dissociates from METTL16 N-terminal domain. **b,c,** RMS fluctuation for each of the residues of the phosphopeptide (pS419) **b** or unmodified METTL16 peptide **c**. **d,e,** RMS deviation in METTL16 N-terminal domain in the presence of a phosphopeptide (pS419) **d** peptide or unmodified Ser419-containing METTL16 **e**. **f,** Immunoblot of phospho-SQ/TQ in HEK293T after transfection of GFP-METTL16 C terminus vector and immunoprecipitation with GFP after indicated treatment. **g,** HEK293T cells were transfected with GFP-METTL16 C terminus WT or S419D vectors and Flag-METTL16 WT N terminus vector. Cell lysates were subjected to immunoprecipitation with Flag beads and immunoblotted with the indicated antibodies. **h,** Immunoblots of METTL16 and Flag in U2OS cells expressing WT, phosphorylation deficient or mimicking mutant (S419A and S419D) GFP-METTL16-Flag. β-Actin was used as a loading control. **i,j,** Representative images **i** and quantification **j** of Duo-link *in situ* in U2OS cells expressing WT or S419D mutation GFP-METTL16-Flag. At least 150 cells were analyzed for each datum point. Data are presented as mean ± SD from three independent experiments (student's t test; ***$p < 0.001$). Scale bar is indicated. **k,** HEK293T cells were transfected with Flag-METTL16 following IR with 10 Gy. Cell lysates were subjected to native-polyacrylamide gel electrophoresis (Native-PAGE) and immunoblot with METTL16 antibody. **l,** HEK293T cells were transfected with Flag-METTL16 WT or 2RE mutant N terminus vectors and GFP-METTL16 WT or S419D C terminus vectors. Cell lysates were subjected to immunoprecipitation with Flag beads and immunoblotted with the indicated antibodies.

Extended Data Fig.6

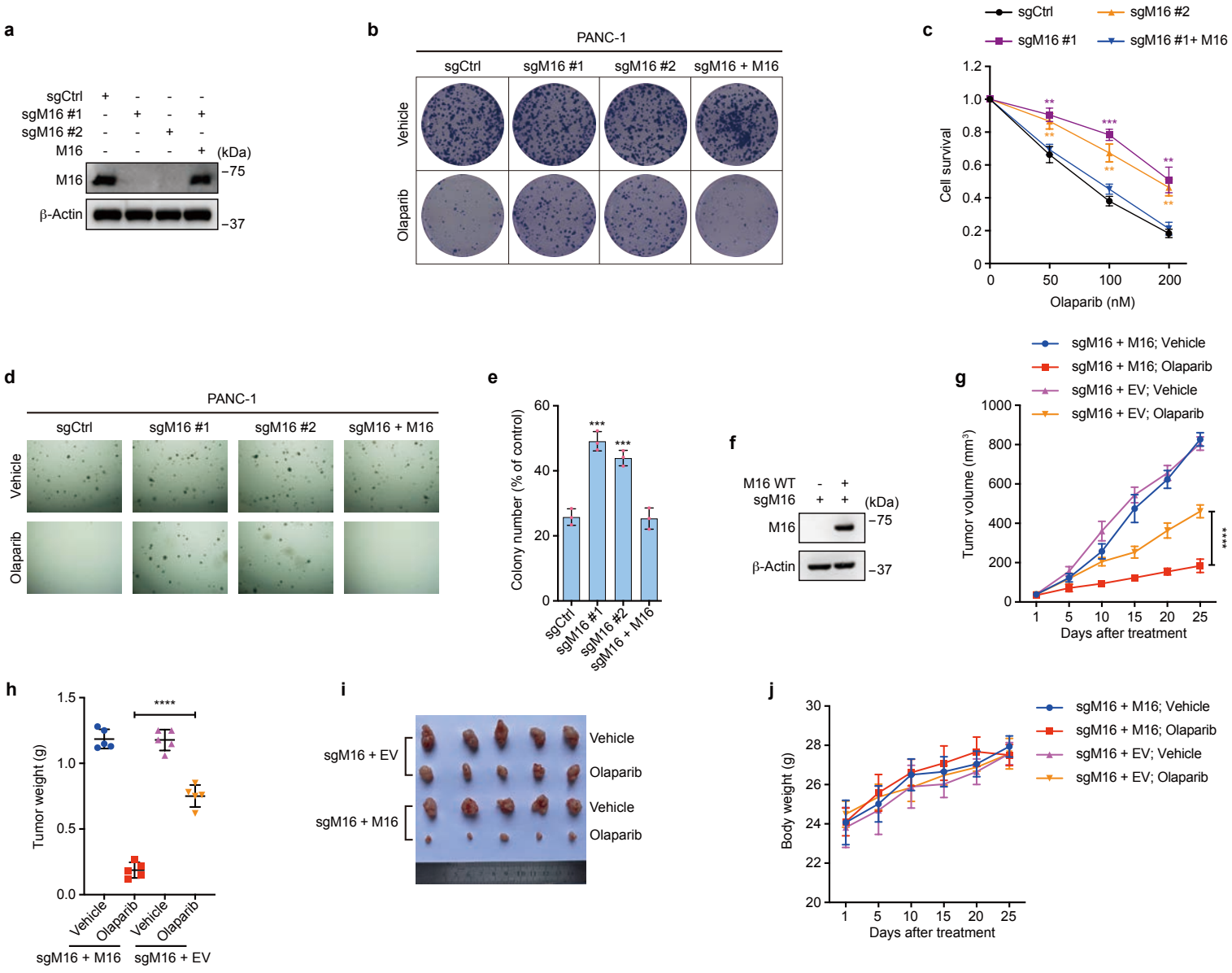

Extended Data Fig. 6 High METTL16 expression is correlated with increased sensitivity to PARPi. a, Immunoblot of METTL16 in METTL16 KO PANC-1 cells re-expressed WT METTL16. β-Actin was used as a loading control. **b,c,** Representative images **b** and quantification **c** of 2-D colony formation assay in the indicated PANC-1 cells treated with olaparib. Data are presented as mean ± SD from three independent experiments (two-way ANOVA; **p < 0.01, ***p < 0.001). **d,e,** Representative images **d** and quantification **e** of soft agar colony formation in the indicated PANC-1 cells treated with olaparib. Data are presented as mean ± SD from three independent experiments (student's t test; ***p < 0.001). **f,** Immunoblot of METTL16 in METTL16 KO SW1990 cells re-expressed empty vector or WT METTL16. β-Actin was used as a loading control. **g,** Growth curves of the SW1990 xenograft tumor models. METTL16-KO cells and METTL16 re-expressing SW1990 cells were injected subcutaneously. When tumors reached approximately 100 mm^3, mice were randomly assigned to treatment with vehicle or olaparib (n = 5 for each group). Data are presented as mean ± SD (two-way ANOVA; ****p < 0.0001). **h,** Quantification of the weight of the tumors in different groups of the xenograft tumor models. Data are presented as mean ± SD (student's t test; ****p < 0.0001). **i,** Photograph of the tumors harvested at the end of the experiment with the SW1990 xenograft tumor models. **j,** Body weight of the mice in different groups of the SW1990 xenograft tumor models.

Extended Data Fig.7

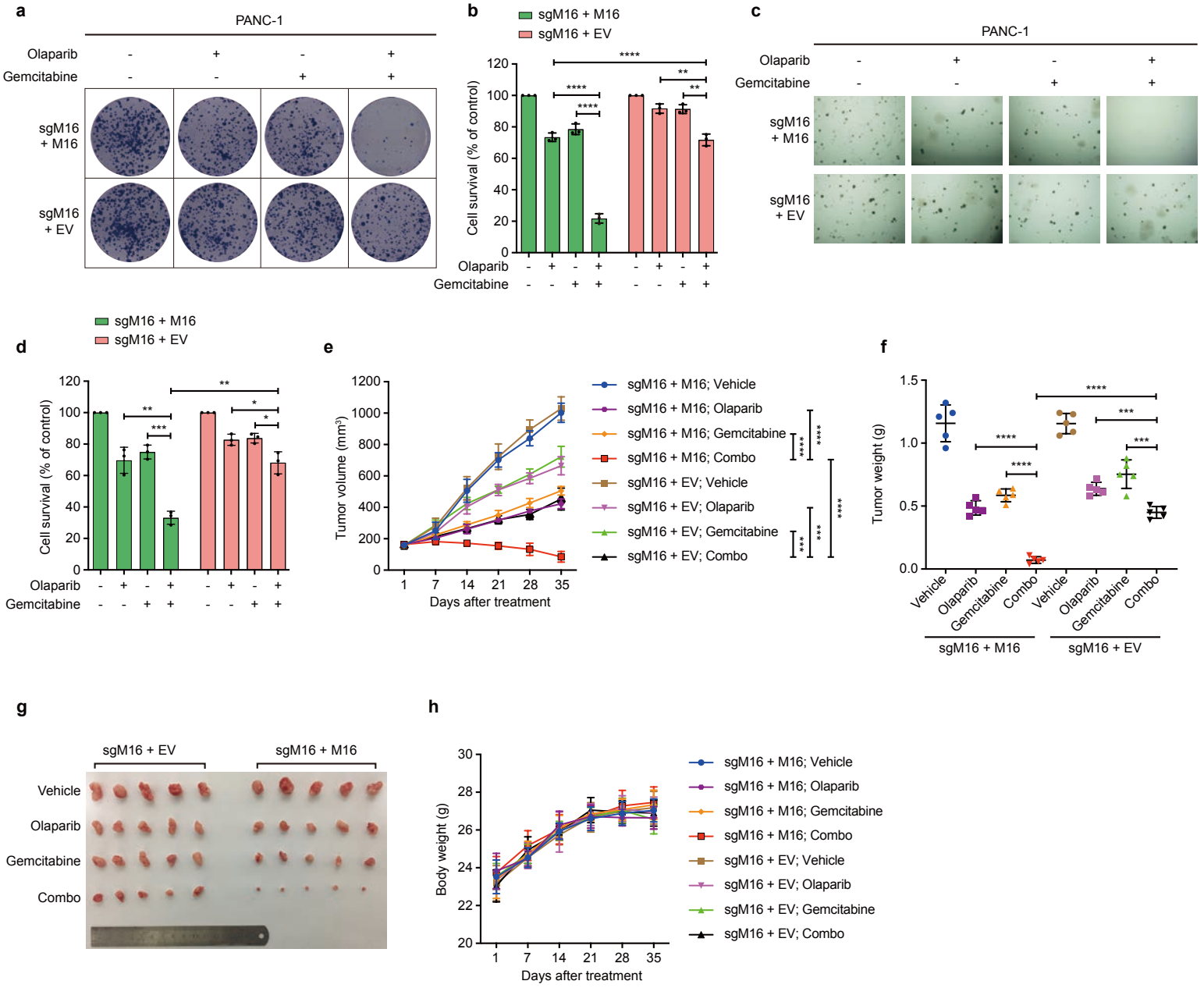

Extended Data Fig. 7 PARPi and Gemcitabine in combination effectively kill tumor cell-expression METTL16. a,b, Representative images **a** and quantification **b** of 2-D colony formation assay in the indicated PANC-1 cells treated with olaparib or gemcitabine. Data are presented as mean ± SD from three independent experiments (two-way ANOVA; $^{**}p < 0.01$, $^{****}p < 0.0001$). **c,d,** Representative images **c** and quantification **d** of soft agar colony formation in the indicated PANC-1 cells treated with olaparib or gemcitabine. Data are presented as mean ± SD from three independent experiments (student's t test; $^{*}p < 0.05$, $^{**}p < 0.01$, $^{***}p < 0.001$). **e,** Growth curves of the SW1990 xenograft tumor models. METTL16-KO cells and METTL16 re-expressing SW1990 cells were injected subcutaneously. When tumors reached approximately 200 mm^3, mice were randomly assigned to treatment with vehicle, olaparib, gemcitabine or combo (n = 5 for each group). Data are presented as mean ± SD (two-way ANOVA; $^{***}p < 0.001$, $^{****}p < 0.0001$). **f,** Quantification of the weight of the tumors in different groups of the xenograft tumor models. Data are presented as mean ± SD (student's t test; $^{***}p < 0.001$, $^{****}p < 0.0001$). **g,** Photograph of the tumors harvested at the end of the experiment with the SW1990 xenograft tumor models. **h,** Body weight of the mice in different groups of the SW1990 xenograft tumor models.